THE JOURNAL OF BIOLOGICAL CHEMISTRY
Vol. 278, No. 5, Issue of January 31, pp. 3137–3144, 2003
Printed in U.S.A.

Isolation, Structure, and Activity of GID, a Novel α4/7-Conotoxin with an Extended N-terminal Sequence*

Received for publication, October 8, 2002
Published, JBC Papers in Press, November 4, 2002, DOI 10.1074/jbc.M210280200

Annette Nicke‡§¶, Marion L. Loughnan‡, Emma L. Millard‡§, Paul F. Alewood‡, David J. Adams§, Norelle L. Daly‡, David J. Craik‡‖, and Richard J. Lewis‡§**

From the ‡Institute for Molecular Bioscience and §School of Biomedical Sciences, University of Queensland, Brisbane, Queensland 4072, Australia

Using assay-directed fractionation of *Conus geographus* crude venom, we isolated α-conotoxin GID, which acts selectively at neuronal nicotinic acetylcholine receptors (nAChRs). Unlike other neuronally selective α-conotoxins, α-GID has a four amino acid N-terminal tail, γ-carboxyglutamate (Gla), and hydroxyproline (O) residues, and lacks an amidated C terminus. GID inhibits its α7 and α3β2 nAChRs with IC_{50} values of 5 and 3 nM, respectively and is at least 1000-fold less potent at the α1β1γδ, α3β4, and α4β4 combinations. GID also potently inhibits the α4β2 subtype (IC_{50} of 150 nM). Deletion of the N-terminal sequence (GIDΔ1–4) significantly decreased activity at the α4β2 nAChR but hardly affected potency at α3β2 and α7 nAChRs, despite enhancing the off-rates at these receptors. In contrast, Arg^{12} contributed to α4β2 and α7 activity but not to α3β2 activity. The three-dimensional structure of GID is well defined over residues 4–19 with a similar motif to other α-conotoxins. However, despite its influence on activity, the tail appears to be disordered in solution. Comparison of GID with other α4/7-conotoxins which possess an NN(P/O) motif in loop II, revealed a correlation between increasing length of the aliphatic side-chain in position 10 (equivalent to 13 in GID) and greater α7 *versus* α3β2 selectivity.

Neuronal nicotinic acetylcholine receptors (nAChR)[1] represent important targets for the development of novel drugs for the treatment of pain and various disorders of the central nervous system (1). To date, eight α and three β subunits (α2–α7, α9, α10, β2–β4) of the nAChRs have been cloned from sensory and neuronal mammalian cells (2–4). For the α7 and α9 subunits, it has been shown that they need no additional subunits to form functional ion channels upon heterologous expression. All other α subunits, however, require at least the co-expression of one β subunit, or another α subunit in the case of α10. Ternary combinations of two different α and one β subunit or two different β and one α subunit, and even quaternary combinations have been described (5, 6). This diversity of subunit combinations has the potential to generate a wide range of receptor subtypes with different pharmacological and functional properties. To help unravel which native neuronal nAChR subunit combinations are responsible for specific physiological functions, additional selective inhibitors are required.

Conotoxins are small disulfide-rich peptides from the venom of the predatory marine snails of the genus *Conus*. These mini-proteins have proved to be valuable tools for investigating the structure and function of ligand- and voltage-gated ion channels. α-Conotoxins are competitive antagonists of acetylcholine (ACh) binding to the nAChR (7). The α-conotoxins described so far are among the most selective inhibitors to be identified (Fig. 1). They are typically 12–18 amino acids long, contain a conserved Pro in loop I, and are folded by two disulfide bonds connecting Cys^1–Cys^3 and Cys^2–Cys^4. Based on the number of amino acids between the second and third cysteine residues (loop I) and the third and fourth cysteine residues (loop II) they are divided into α3/5, α4/7, α4/6, and α4/3 structural subfamilies (8). The α3/5-conotoxins are selective for the muscle-type nAChR, while most α4/7- and α4/6-conotoxins are selective for neuronal nAChRs. An exception is the α4/7-conotoxin EI, which binds to the α/δ interface of the muscle-type nAChR (9). The α4/3-type characterized by ImI is α7-selective (10). The three-dimensional structures of different neuronal-specific and muscle-specific α-conotoxins have been determined by NMR (11–15) and x-ray structural analysis (16–19). The α4/7-conotoxins and ImI share similar backbone conformations and a rigid hydrophobic core (14), suggesting that their different specificities for nAChR subtypes arise from the different amino acid side-chains projecting from this conserved scaffold.

The α4β2 nAChRs together with the α7 subtype are the most abundant nAChRs in mammalian brain. Knockout studies in mice have revealed an important role for α4 and β2 in pain and cognition (20) but further investigations of its role are limited by the lack of α4β2-selective inhibitors. A primary goal of this study was to identify new α-conotoxins active at the α4β2 subtype. In this report, we describe the isolation and characterization of α4/7-conotoxin GID. GID possesses a novel four amino acid N-terminal tail and an Arg in position 12 that contribute to α4β2 selectivity. The NMR structure of GID was determined to define the location of structural features that contribute to the selectivity of GID.

* This study was supported by Australian Research Council Discovery Grant DP0208295 and by an Australian Research Council Special Research Center for Functional and Applied Genomics. The costs of publication of this article were defrayed in part by the payment of page charges. This article must therefore be hereby marked "*advertisement*" in accordance with 18 U.S.C. Section 1734 solely to indicate this fact.

The atomic coordinates and structure factors (code 1MTQ) have been deposited in the Protein Data Bank, Research Collaboratory for Structural Bioinformatics, Rutgers University, New Brunswick, NJ (http://www.rcsb.org/).

¶ Supported by Research Fellowship NI 592/2-1 of the Deutsche Forschungsgemeinschaft.

‖ An ARC Professorial Fellow.

** To whom correspondence should be addressed: Inst. for Molecular Bioscience, University of Queensland, Brisbane, QLD 4072, Australia. Tel.: 61-7-3365-1924; Fax: 61-7-3365-1990; E-mail: r.lewis@imb.uq.edu.au.

[1] The abbreviations used are: nAChR, nicotinic acetylcholine receptors; ACh, acetylcholine; α-GID, α-conotoxin GID; α-PnIA, α-conotoxin PnIA; γ, γ-carboxyglutamic acid (Gla); O, hydroxyproline (Hyp); RMSD, root mean-squared deviation; RP-HPLC, reverse phase-high performance liquid chromatography.

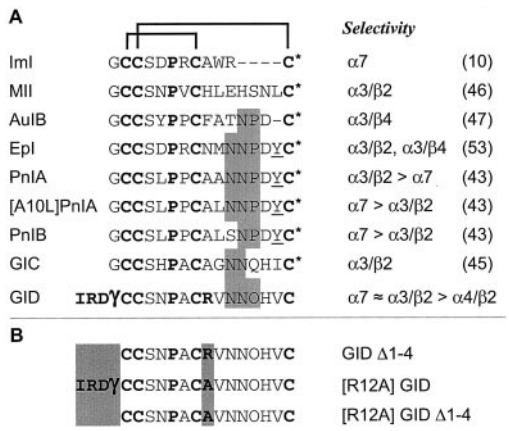

FIG. 1. **Comparison of α-GID and related neuronally active α-conotoxins.** *A*, sequence and selectivity of neuronally active α-conotoxins. A motif (NN(O/P)) commonly found in the second loop of α4/7-conotoxins is marked in *gray*. *Asterisks* indicate C-terminal amidation. Sulfated Tyr are *underlined*, γ, γ-carboxyglutamic acid, and O, hydroxyproline. *B*, sequences of GID analogues investigated in this study. Mutated residues are marked in *gray*. Selectivity determined from oocyte studies except for EpI, which was determined from studies in neurons.

EXPERIMENTAL PROCEDURES

Isolation, Purification, and Sequencing of GID

Extraction of Crude Venom—Nine specimens of *Conus geographus* were collected from the Great Barrier Reef, Australia. Crude venom duct contents were extracted with 30% acetonitrile/water acidified with 0.1% trifluoroacetic acid and centrifuged. Soluble material (120 mg) was lyophilized and stored at −20 °C prior to use.

Isolation and Purification of GID—A portion of the crude venom extract (40 mg) was fractionated on a semipreparative RP-HPLC column (10-μm C_{18}, Vydac) eluted at 3 ml/min with a linear gradient of 0–80% solvent B over 80 min (solvent A, 0.1% trifluoroacetic acid; solvent B, 90% acetonitrile, 0.09% trifluoroacetic acid). Inhibition in a functional nAChR assay (see below) identified an active 1-min fraction eluting at ~21 min (Fig. 2*A*), which was further purified by RP-HPLC employing a linear gradient of 0–25% B over 25 or 45 min (5-μm C_{18}, 46 × 250 mm Zorbax or Jupiter columns at 1 ml/min or a SB300 3.5 μm C_{18}, 2.1 × 50 mm Zorbax column at 0.2 ml/min eluted with solvent A, 0.05% trifluoroacetic acid; solvent B, 90% acetonitrile and 0.045% trifluoroacetic acid). An active peptide detected at 214 nm was collected and sequenced after reduction and alkylation with maleimide (see below). Venom was further characterized by LC/MS analysis using a PESciex API QSTAR Pulsar mass spectrometer (m/z 500–2200) to monitor the eluant from a 5-μm C_3, 2.1 × 150 mm Zorbax column eluted with 0–60% B over 60 min (A, 0.1% formic acid; B, 90% aqueous acetonitrile, 0.09% formic acid).

Sequencing—The purified peptide (~20 pmol) was reduced in the presence of 10 mM TCEP and 50 mM ammonium acetate, pH 4.5 (37 °C for 1 h) before alkylating in the added presence of 20 mM maleimide (37 °C for 1 h). The alkylated peptide was repurified by RP-HPLC prior to sequence analysis by Edman chemistry on a 492–01 HT model Procise protein sequencer (see Fig. 1). Stock solutions of 100 mM Tris(2-carboxyethyl)-phosphine hydrochloride (Pierce), and maleimide (Aldrich) were prepared in 0.1 M ammonium acetate pH 4.5 and in 10% acetonitrile, respectively, and stored at −20 °C.

Peptide Synthesis

GID and analogues were manually assembled by Boc chemistry, deprotected, and cleaved from resin as described previously (21). Amino acid side-chain protection was as follows: Arg (Tos), Asn(Xan), Asp(O-cHex), Cys(*p*MeBzl), Gla(OcHex), His (DNP), Hyp(Bzl), and Ser(Bzl). Linear peptides were manually assembled on *t*-Boc-cysteine-Pam resin, (0.75 mmol substitution/g; Applied Biosystems, Foster City, CA). Double couplings were used where necessary to achieve coupling efficiencies of >99.5%. HPLC-purified reduced peptides (50 μM) were oxidized in 100 mM ammonium bicarbonate at pH 7.5–8 with stirring for 24–48 h at 23 °C. The oxidized peptides were purified by preparative RP-HPLC. The major oxidized product was co-injected with native GID in a 2:1 ratio. Peptides were quantified initially in triplicate by amino acid analysis (22), then subsequently by RP-HPLC using an external reference standard for each peptide.

Functional Characterization of GID

RNA Preparation—Plasmids containing cDNA encoding rat α3, α4, α7, β2, and β4 nAChR subunits were provided by J. Patrick (Baylor College of Medicine, Houston, TX) and subcloned into the oocyte expression vector pNKS2 (23). cDNAs for the mouse α1, β1, γ, and δ subunits of the muscle nAChR were provided by Dr. V. Witzemann (Max-Planck Institute for Medical Research, Heidelberg, Germany). Capped cRNAs were synthesized from linearized plasmid cDNAs using the Message Machine Kit (Ambion, Austin, TX).

Expression in Xenopus Oocytes—Oocytes were prepared as previously described (24), injected with 50 nl of cRNA (5–50 ng/μl), and kept at 19 °C in ND96 (96 mM NaCl, 2 mM KCl, 1 mM $CaCl_2$, 1 mM $MgCl_2$, and 5 mM Hepes at pH 7.4) supplemented with 50 mg/liter of gentamycin (Sigma Chemical Co.).

Two Electrode Voltage-Clamp Recording—Two electrode voltage-clamp recordings were performed in oocytes 2–10 days after cRNA injection at a holding potential of −70 mV. Pipettes were pulled from borosilicate glass (Harvard Apparatus Ltd., Kent, England) and filled with 3 M KCl. Resistances were below 1 MΩ. Membrane currents were recorded using a two electrode virtual ground circuit on a GeneClamp 500B amplifier (Axon Instruments Inc., Union City, CA), filtered at 200 Hz and digitized at 1 kHz using a Digidata 1322A interface and v8.2 Clampex software (Axon Instruments Inc.). Recordings were performed in ND96 at room temperature. 1 μM ACh (Sigma) was used to activate α4β4 and α1β1γδ nAChRs, 100 μM ACh was used to activate α3β2, α3β4, and α4β2 nAChRs, and 100 μM nicotine (Sigma) was used to activate α7 nAChR. The perfusion medium was manually switched between ND96 with or without agonist using a Valve Driver II (General Valve Corporation, Fairfield, NJ). A fast and reproducible solution exchange (<300 ms) for agonist application was achieved using a 50-μl funnel-shaped oocyte chamber combined with a fast solution flow (~150 μl/s) fed through a custom-made manifold mounted immediately above the oocyte. ACh pulses were applied for 2 s at 6-min intervals. After each application, the cell was superfused for 1 min with agonist-free solution, and the flow was then stopped for 5 min before agonist solution was re-introduced. Peptide was applied when responses to three consecutive agonist applications differed by less than 10%. After the 1-min agonist washout step was stopped, 5.5 μl of a 10-fold concentrated peptide solution were pipetted directly into the static bath, mixed by repeated pipetting, and incubated for 5 min prior to application of agonist. Addition of toxin directly to the recording chamber conserved material and avoided potential adhesion of the toxin to tubing surfaces. To obtain estimates of potency, dose-response curves were fitted to the data by the equation percent response = $100/\{1 + ([\text{toxin}]/IC_{50})^{nH}\}$ using Prism software (GraphPad v 3.0 for Macintosh, San Diego, CA). To obtain estimates of toxin washout kinetics, agonist responses were measured at 2-min intervals under constant superfusion. For toxin application, oocytes were superfused for 1 min before a 1-min incubation with the toxin followed by the next agonist application.

NMR Solution Structure of GID

Sample Preparation—Samples for ^{1}H NMR measurement contained ~2.5 mM synthetic GID in 90% H_2O, 10% D_2O or 100% D_2O at pH 2.8.

NMR Spectroscopy—Spectra were obtained on a Bruker DMX 750 spectrometer at 280 and 287 K. All spectra were acquired in phase-sensitive mode using TPPI (25). The homonuclear spectra recorded included double quantum filtered DQF-COSY (26), TOCSY (27) using a MLEV17 spin lock sequence (28) with an isotropic mixing time of 80 ms; ECOSY (29), and NOESY (30) with mixing times of 150 and 350 ms. In DQF-COSY and ECOSY experiments, the water resonance was suppressed by low power irradiation during the relaxation delay (1.5 s). For the TOCSY and NOESY experiments, water suppression was achieved using a modified WATERGATE sequence (31). Two-dimensional spectra were generally collected over 4096 data points in the f2 dimension and 512 increments in the f1 dimension over a spectral width corresponding to 12 ppm. For identification of slowly exchanging amides, a series of one-dimensional and TOCSY spectra were run immediately after dissolving the sample in D_2O. All spectra were processed on a Silicon Graphics workstation using XWINNMR (Bruker). The f1 dimension was zero-filled to 2048 real data points with the f1 and f2 dimensions being multiplied by a sine-squared function shifted by 90° prior to Fourier transformation. Processed spectra were analyzed and assigned using the program XEASY (32). Spectra were assigned using the sequential assignment protocol (33). The process was facilitated, in part,

using the automatic assignment program NOAH, which is part of the DYANA package (34).

Structure Calculations—Cross-peaks in NOESY spectra recorded in 90% H_2O, 10% D_2O with mixing times of 350 and 150 ms were integrated and calibrated in XEASY, and distance constraints were derived using DYANA. Backbone dihedral angle restraints were derived from $^3J_{HNH\alpha}$ coupling constants measured from line shape analysis of antiphase cross-peak splitting in the DQF-COSY spectrum. Angles were restrained to $-120° \pm 30$ for $^3J_{HNH\alpha} > 8.5$ Hz and to $-60° \pm 30$ for $^3J_{HNH\alpha} < 5$ Hz. Stereospecific assignments of β-methylene protons and χ1 dihedral angles were derived from $^3J\alpha\beta$ coupling constants, measured from ECOSY spectra, in combination with NOE peak intensities (35). Slowly exchanging amide protons identified by D_2O exchange experiments were used in conjunction with preliminary structures to determine hydrogen bonds. In cases where hydrogen bonds could be determined and unambiguously assigned, appropriate distance restraints were included in the subsequent calculations. Preliminary structures were calculated using a torsion angle simulated annealing protocol within DYANA. Final structures were calculated using simulated annealing and energy minimization protocols within CNS version 1.0 (36). The starting structures were generated using random ϕ, ψ dihedral angles and energy-minimized to produce structures with the correct local geometry. A set of 50 structures was generated by a torsion angle simulated annealing protocol (37, 38). This protocol involves a high temperature phase comprising 4000 steps of 0.015 ps of torsion angle dynamics, a cooling phase with 4000 steps of 0.015 ps of torsion angle dynamics during which the temperature was lowered to 0 K, and finally an energy minimization phase comprising 5000 steps of Powell minimization. Structures consistent with restraints were subjected to further molecular dynamics and energy minimization in a water shell, as described by Linge and Nilges (39). The refinement in explicit water involves the following steps. First heating to 500 K via steps of 100 K, each comprising 50 steps of 0.005 ps of Cartesian dynamics. Second, 2500 steps of 0.005 ps of Cartesian dynamics at 500 K before a cooling phase where the temperature was lowered in steps of 100 K, each comprising 2500 steps of 0.005 ps of Cartesian dynamics. Finally, the structures were minimized with 2000 steps of Powell minimization. Structures were analyzed using Promotif and Procheck (40, 41).

RESULTS

Isolation and Chemical Characterization of GID

Isolation and Sequence of GID—In the search for new α-conotoxins, the crude venom of *C. geographus* was screened for inhibition of agonist-evoked currents at muscle nAChR and different combinations of neuronal nAChR subunits (α3β2, α3β4, α4β2, α4β4, and α7) heterologously expressed in *Xenopus* oocytes. Crude venom (50 μg protein/ml by BCA assay) caused 100% block of the α3β2 and α7 nAChR subtypes and had weak activity at α4β2. LC/MS analysis of the crude venom, and MS analysis of individual fractions, confirmed the presence of the known muscle selective α-conotoxins GI, GIA, and GIB, while GII and the neuronally active GIC were not found (Fig. 2, *A* and *B*). Thus this pool of *C. geographus* crude venom appeared to contain a novel neuronally active α-conotoxin. Inhibitory activity at the α3β2 and α7 subtypes was used to guide fractionations of the crude venom, yielding a single component of 2184.9 Da (Fig. 2, *A* and *B*) that inhibited α3β2, α7, and α4β2 nAChR subtypes. Edman sequencing of the reduced and alkylated peptide, together with mass spectrometry evidence for the γ-carboxyglutamic acid (γ), revealed a new α4/7-conotoxin sequence IRDγCCSNPACRVNNOHVC (Fig. 1), that we named α-GID following the nomenclature proposed by Olivera and co-workers (8). The identical sequence was also identified in *Conus tulipa* crude venom.[2] GID possesses an NN(P/O) motif also found in α-conotoxins EpI, PnIA, and PnIB (Fig. 1*A*) but additionally has a four residue N-terminal tail. GID is the first non-amidated, neuronally active α-conotoxin identified.

Chemical Synthesis of GID and Analogues—To characterize GID and investigate the influence of the N-terminal tail on its functional properties, GID and an analogue missing the four

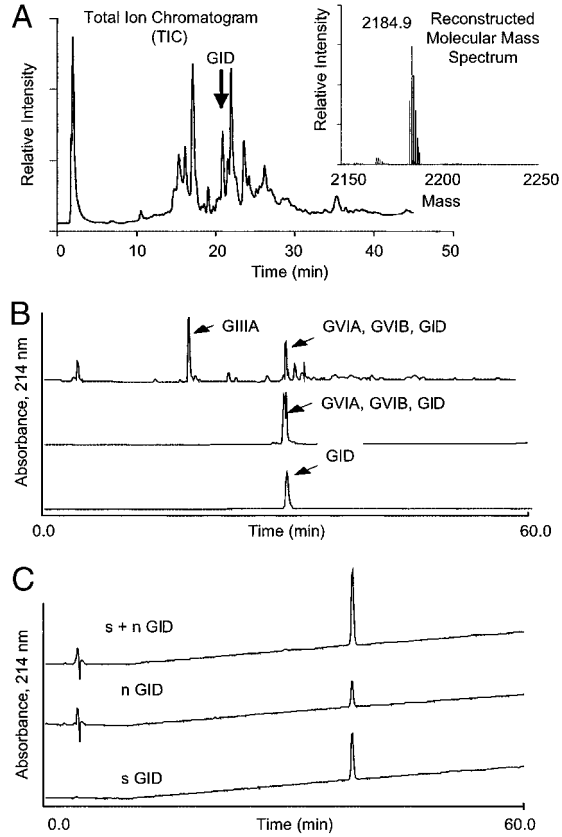

FIG. 2. **Isolation and synthesis of α-GID.** *A*, total ion chromatogram of *C. geographus* crude venom extract. The *arrow* indicates α-GID. A reconstructed molecular mass spectrum of GID is shown in the *inset*. *B*, purification of GID by HPLC. *C*, coelution of native and synthetic GID. Synthetic GID (*sGID*) and native (*nGID*) were co-injected in a 2:1 ratio and analyzed by HPLC. Retention time (38.3 min) and peak width was the same for synthetic, native, and the co-injected peptides.

N-terminal amino acids (GIDΔ1–4) were synthesized (Fig. 1*B*). A single point mutant, [R12A]GID, was also synthesized to investigate the influence of the unusual charged residue in this position on nAChR selectivity. All peptides were purified to >95% purity determined by HPLC and MS analysis. Oxidized synthetic GID co-eluted with native GID on reversed-phase HPLC (Fig. 2*C*), and both peptides had identical masses (monoisotopic masses: observed native, 2184.9; observed synthetic, 2184.9; theoretical, 2184.9).

Functional Characterization of GID—Both native and synthetic GID blocked α3β2 and α7 nAChRs receptors expressed in *Xenopus* oocytes with equal potency (data not shown). Synthetic GID was used in further experiments to determine the potency and subtype selectivity of GID at neuronal α3β2, α3β4, α4β2, α4β4, and α7, and muscle α1β2γδ nAChRs expressed in oocytes. The concentration response curves for GID are shown in Fig. 4*A*, and IC_{50} values and Hill slope coefficients are summarized in Table I. GID was most potent at α3β2 and α7 nAChR subtypes, with IC_{50} values of 3 and 5 nM, respectively (Fig. 3*A*). The activity at the α3β4, α4β4, and muscle nAChRs was at least 1000-fold less. This potency and selectivity profile of GID is somewhat reminiscent of α-conotoxin PnIA and [A10L]PnIA (42, 43). In contrast to these peptides, however, GID also showed activity at the α4β2 subtype (IC_{50} 150 nM). Despite several sequence similarities in the second loop, no α4β2 activity was found for [A10L]PnIA (42) at 3 μM (Fig. 3*B*).

Influence of the N-terminal Tail and Arg[12] on Subtype Selectivity—To identify which structural determinants contribute to GID selectivity, the roles of the N-terminal tail and the basic residue Arg^{12} were investigated. Deletion of the four N-termi-

[2] L. Thomas and R. J. Lewis, unpublished data.

TABLE I
Inhibition of nAChR currents by α-GID and analogues

IC_{50} values (nM) and Hill slopes ($-n_H$) for inhibition of agonist-evoked current through $\alpha3\beta2$, $\alpha4\beta2$, and $\alpha7$ subtypes expressed in Xenopus oocytes are shown.

α-Conotoxin	α3β2	α4β2	α7
GID	3.1 (1.16)	152 (1.13)	4.5 (1.06)
GIDΔ1–4	4.6 (1.07)	670 (1.16)	5.5 (1.15)
[R12A]GID	10 (1.14)	2000 (0.86)	48 (1.26)

nal amino acids of GID reduced the activity of the peptide at the $\alpha4\beta2$ combination by ~4-fold (Fig. 3*B*). Interestingly, GIDΔ1–4 (1–10 μM) caused only a partial block (~40%) of $\alpha4\beta2$ receptors, indicating that the tail of GID was required for full antagonist activity at this subtype combination (no partial agonist activity was detected with this truncated analogue, data not shown). However, potency at the $\alpha7$ and $\alpha3\beta2$ subtypes was little influenced by removal of the four N-terminal residues. Activity of [R12A]GID at the $\alpha4\beta2$ and $\alpha7$ subtype was reduced ~10-fold compared with GID, whereas activity at the $\alpha3\beta2$ subtype was little affected (Fig. 3, *B–D*). An analogue in which the four N-terminal amino acid residues of [R12A]GID were removed ([R12A]GIDΔ1–4) did not cause any inhibition of the $\alpha4\beta2$ receptor at 3 μM (data not shown).

Influence of the N-terminal Sequence on the Off-rate Kinetics—Inhibition of the $\alpha4\beta2$ nAChR by GID and its analogues was rapidly reversible, with at least 90% recovery of responses seen after 2 min (data not shown). However, recovery of the $\alpha3\beta2$ and $\alpha7$ subtypes from GID block was significantly slower, requiring 10 and 15 min, respectively (Fig. 4, *A* and *C*). In contrast, inhibition of both $\alpha3\beta2$ and $\alpha7$ receptors by GIDΔ1–4 was reversed after a <2-min washout (Fig. 4, *B* and *D*). Recovery from block by [A10L]PnIA, which does not have an N-terminal tail, was rapid at the $\alpha3\beta2$ subtype but slow at the $\alpha7$ subtype (data not shown).

Structural Characterization of GID

NMR Assignments—All spectral data on GID were recorded in either 90% H_2O, 10% D_2O or 100% D_2O. Spectra recorded at 287 K were primarily used for assignments, while spectra measured at other temperatures were used to resolve ambiguities.

Structure Determination and Analysis—Analysis of the 350-ms NOESY spectrum (750 MHz, 287 K) using the program XEASY allowed the assignment of each spin system to a specific amino acid. All non-intraresidual peaks were subsequently assigned both manually and using the NOAH automatic assignment within the DYANA program package. Interproton distance restraints were derived from the NOE intensities and used in structure calculations using a torsion angle simulated annealing protocol within DYANA. Preliminary structures were analyzed to resolve spectral ambiguities and to facilitate the introduction of new restraints. A set of restraints consisting of 183 NOE-derived distances and 15 dihedral angle restraints was used in the final calculations. These restraints included 82 sequential, 35 medium range, 10 long range, and 56 intraresidue distances, 6 ϕ angle restraints (Cys^5, Cys^6, Arg^{12}, Val^3, His^{17}, and Cys^{19}), and 9 χ_1 angle restraints (Cys^5, Cys^6, Asn^8, Cys^{11}, Val^{13}, Asn^{14}, His^{17}, Val^{18}, and Cys^{19}). Side-chain angle restraints were derived on the basis of coupling constants and NOE intensities from a 150 ms NOESY spectrum. There were also four restraints included for two hydrogen bonds identified in preliminary structures. In the final round of structure calculations, these restraints were used to calculate a family of 50 structures, using a torsion angle simulated annealing (37, 38) protocol within CNS version 1.0 (36). Structures consistent with the restraints were subjected to further molecular dynamics and energy minimization in a water shell.

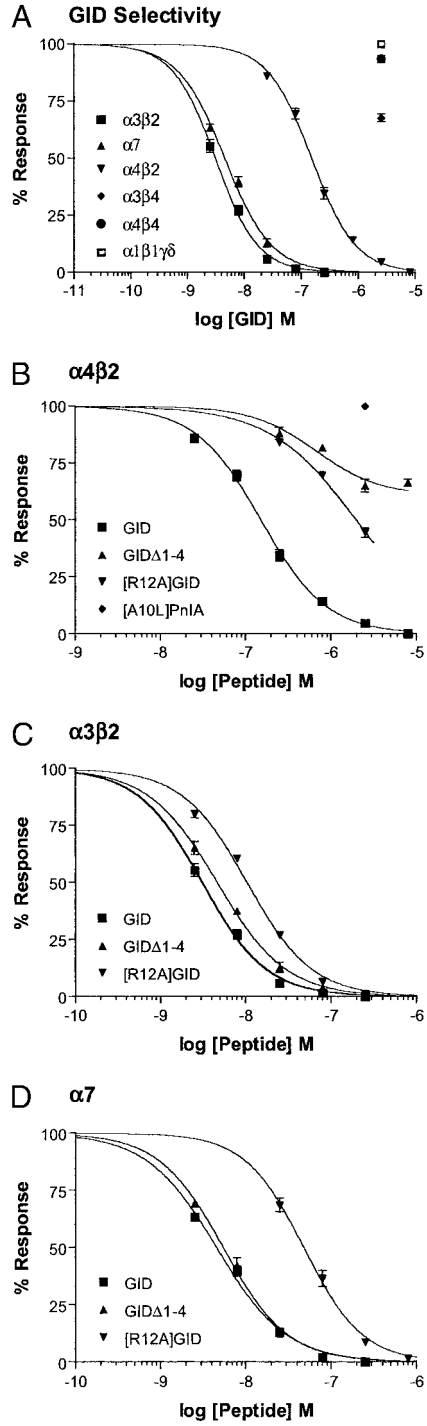

FIG. 3. **Comparison of subtype selectivity and activity of α-GID and its analogues at nAChRs expressed in *Xenopus* oocytes.** Oocytes were injected with cRNA encoding the indicated nAChR subunits and voltage clamped 2–10 days after injection. Responses to ACh or nicotine (for $\alpha7$) after a 5-min incubation in the presence of peptide are shown as percentage of control responses. *Error bars* are S.E. and $n = 3–5$ for each data point. *A*, subtype selectivity of GID. Comparison of inhibition by GID and its analogues at $\alpha4\beta2$ (*B*), $\alpha3\beta2$ (*C*), and $\alpha7$ (*D*) nAChRs. IC_{50} values and Hill slope coefficients are summarized in Table I.

Secondary Structure—The differences between the Hα chemical shifts of GID and random coil values (44) are shown in Fig. 5. A negative secondary shift (upfield) for several residues indicates that GID contains helical structural elements. The longest uninterrupted region of negative secondary shifts is

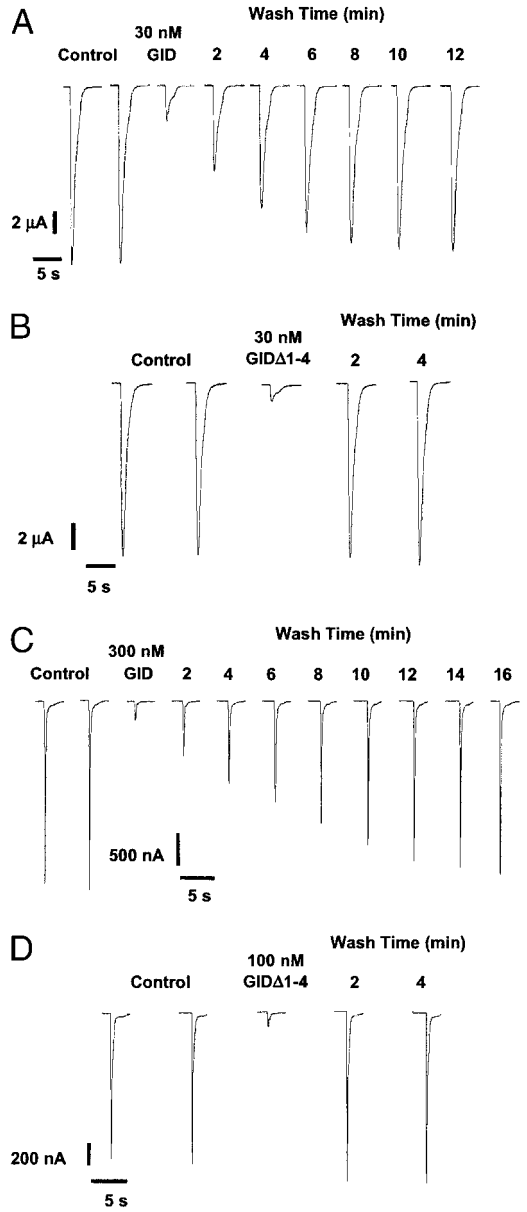

FIG. 4. **Washout kinetics of GID and GIDΔ1–4 from α3β2 and α7 nAChRs.** *Xenopus* oocytes expressing the α3β2 (*A* and *B*) or α7 (*C* and *D*) nAChR subtypes were stimulated with 1-s pulses of ACh or nicotine (in the case of α7) applied at 2-min intervals. Oocytes were first perfused for one more minute with ND96 solution, then incubated with toxin for 1 min in a static bath, before recommencing agonist applications during superfusion. Experiments were repeated three times with similar results. Note that at short incubation times GID is less potent than GIDΔ1–4, indicating that removal of the N-terminal tail increased on-rate kinetics as well as accelerating the off-rate kinetics.

observed for residues 9–13, suggesting that this region forms a well-defined helix.

Disulfide Connectivity—The amino acid sequence of GID includes four cysteine residues that are involved in two disulfide bonds. Initially, the connectivities of the disulfide bonds were unknown but were assumed to be identical to PnIA on the basis of sequence similarities. Thus, the pairing of the disulfides was assumed to be 5–11 and 6–19 (the globular conformation). To test the validity of this assumption, in addition to calculations with the globular connectivity, structures were calculated with the other two possible disulfide connectivities, 5–6, 11–19 (beads conformation), and 5–19, 6–11 (ribbon conformation). The resultant structures for the beads and ribbon isomers clearly violated the experimental data with the average target

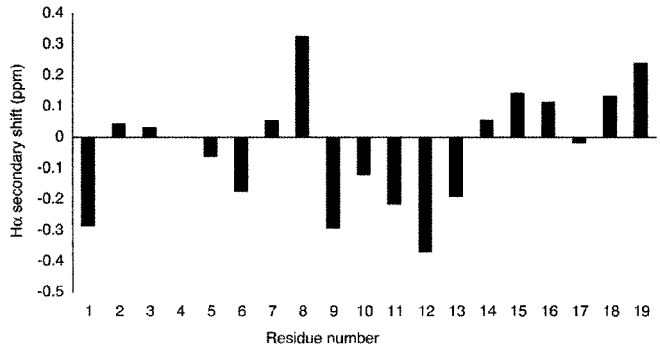

FIG. 5. **Hα chemical shift differences of α-GID from random coil values.**

function from DYANA significantly higher than observed for the globular conformation. The beads and ribbon conformations had target functions of 17.45 and 13.44, respectively, compared with 0.16 for the globular conformation. Structures were also calculated without S–S restraints, and the average target function was 6.94. Analysis of the S-S distances in these structures revealed Cys^5–Cys^{11} was the most likely connectivity. The next most likely bond was between Cys^6–Cys^{19}; however, the distance between Cys^5–Cys^{19} was not significantly different. In summary, the structure calculations with and without the disulfide bonds confirmed that GID adopted the globular conformation, and thus had the same disulfide bond pairings as other α-conotoxins.

Description of the Three Dimensional Structure of GID—A family of the 20 lowest NOE energy structures was chosen from the final set of 50 structures to represent the solution structure of GID. The statistics for these 20 structures, which had no distance violations greater than 0.2 Å and no dihedral angle violations greater than 3.0°, are given in Table II. The structures were well defined with the exception of the N-terminal tail, which had few experimental restraints defining this region. The mean RMSD over residues 4–19 was 0.34 ± 0.17 Å for the backbone atoms and 1.43 ± 0.32 Å for the heavy atoms. The family of structures obtained superimposed over the backbone atoms of residues 4–19 is shown in Fig. 6*A*. The ribbon representation of the lowest energy structure is shown in Fig. 6*B*. Analysis of the backbone angles reveals that 85% of the residues lie in the most favorable regions of the Ramachandran plot, 14% are in the additionally allowed region, 0.5% in the generously allowed region, and 0.5% in the disallowed region. The residues in the generously allowed and the disallowed regions correspond to Asp^3 and Ile^1, respectively, both in the poorly defined N-terminal tail.

The solution structure of GID was determined to be a highly compact globular structure consisting of a central region of α-helix and β-turns at both the N and C termini. The α-helix comprises residues 9–13 and has two turns. H-bonds between Asn^8(O)–Cys^{11}(HN) and Pro^9(O)–Val^{13}(HN) were deduced from analysis of preliminary structures and slow exchange data and were explicitly included in the structure calculations. At the N terminus, the poor definition of residues 1–3 may be associated with flexibility of this region in solution. Analysis with PROMOTIF reveals that residues 5–8 are involved in a type I β-turn, while residues 15–18 are involved in a type II β-turn in 7 of 20 final structures.

A surface representation of GID illustrates a distinct hydrophobic face (Fig. 7*A*) comprising residues Pro^9, Ala^{10}, Val^{13}, Hyp^{16}, and Val^{18}. The hydrophilic residues on the surface include Ser^7, Asn^8, Asn^{14}, and Asn^{15}. There are also four charged residues on the surface of the molecule. Three (Arg^2, Asp^3, and Gla^4) are part of the disordered N-terminal

TABLE II
Geometric and energy statistics for the 20 final structures of α-GID

RMSD from experimental restraints	
Interproton distances (Å)	0.036 ± 0.001
Dihedral angles (deg)	0.28 ± 0.26
RMSD from idealized geometry	
Bonds (Å)	$3.90 \times 10^{-3} \pm 0.0002$
Angles (deg)	0.58 ± 0.02
Impropers (deg)	0.51 ± 0.03
Energies (kcal mol^{-1})	
E_{total}	−601 ± 37.2
E_{NOE}	10.9 ± 1.1
E_{cdih}	0.13 ± 0.23
E_{vdw}	−16.9 ± 5.9
$E_{bond} + E_{angle} + E_{improper}$	36.1 ± 3.17
Pairwise RMSD for backbone atoms (N,Cα,C) (Å)	
Residues 4–19	0.34 ± 0.17
Pairwise RMSD for heavy atoms (Å)	
Residues 4–19	1.43 ± 0.32
Number of NOE derived inter-residual distance restraints	
Sequential	82
Medium range	35
Long range	10
Intraresidue	56
Total	183
Number of dihedral angle restraints	
Phi (ϕ)	6
Chi1 (χ_1)	9
Total	15
Ramachandran plot (%)	
Favorable region	85
Additionally allowed	14
Generously allowed	0.5
Disallowed	0.5

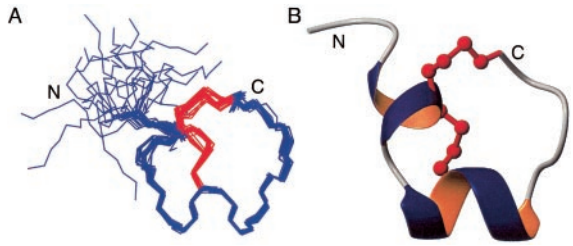

FIG. 6. **The three-dimensional structure of α-GID.** *A*, a family of 20 GID structures superimposed over the backbone atoms of residues 4–19. The disulfides are shown in *red* and the N and C termini are labeled. *B*, secondary structure of GID showing the α-helix, two β turns between residues 4–7 and 14–17, and the tail region. The N and C termini are labeled. The coordinates for α-GID have been deposited with the Research Collaboratory for Structural Bioinformatics Protein Data bank (PDB 1MTQ).

tail. The fourth (Arg^{12}) is situated adjacent to the hydrophobic face.

DISCUSSION

Using functional nAChR assay-guided fractionation, we isolated α-conotoxin GID from the crude venom of *C. geographus*. α-GID is the sixth α-conotoxin and the second neuronally active α-conotoxin isolated from this species (8, 45), showing the importance of α-conotoxins targeting both muscle and neuronal nAChRs for prey capture. GID appears to replace GIC in this pool of *C. geographus* venom. The sequence of GID differs from previously described α-conotoxins in a number of regards. The most striking is the novel N-terminal tail comprising four amino acids (Ile^1, Arg^2, Asp^3, Gla^4) including the post-translationally modified γ-carboxyglutamic acid (Gla). An examination of the pre-pro regions of α-conotoxins from the SWISS-PROT data base reveals that most conopeptide precursor sequences contain Arg-Arg, Lys-Lys, Gln-Arg, Lys-Arg, or Arg-Asp motifs as the cleavage site. For example, ImIIA utilizes Ile-Arg-Asp-Tyr (accession number Q9U619) to leave a Tyr at position 1 in the mature conopeptide. Since the Arg-Asp cleavage site is not utilized in GID, it appears that the γ-carboxylation of Glu4 in GID inhibits this cleavage site, allowing the N-terminal tail to survive in the venom. GID is the first α-conotoxin to utilize a hydroxyproline residue, despite its widespread use in other classes of conotoxins, and is the first neuronally active α-conotoxin with a non-amidated C terminus.

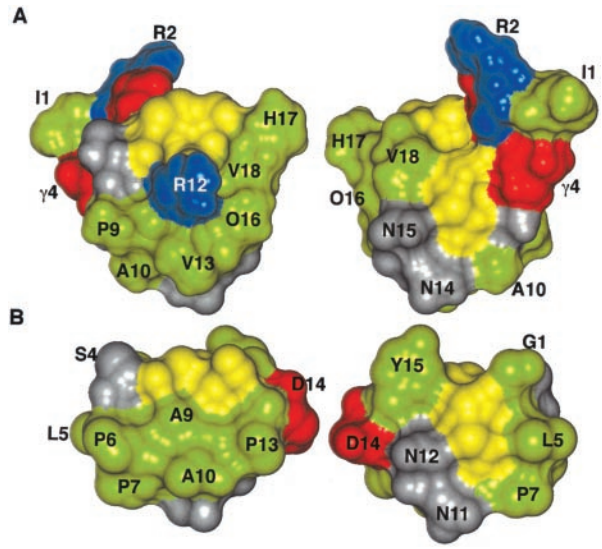

FIG. 7. **Comparison of the surfaces of α-GID (*A*) and PnIA (*B*).** Two orientations (rotated 180° around the *y*-axis) are shown for each molecule superimposed over the α-helical residues. Negatively and positively charged residues are shown in *red* and *blue*, respectively (the His is assumed to be uncharged at physiological pH). Hydrophobic residues are shown in *green*, and hydrophilic residues are in *gray*. Cysteine residues involved in disulfide bonds are shown in *yellow*. Note a common hydrophobic patch comprising Pro^6, Pro^7, Ala^{10}, and Pro^{13} in PnIA, and Pro^9, Ala^{10}, Val^{13}, and Hyp^{16} in GID.

Several neuronally active α-conotoxins have been identified that have nanomolar potency for only the α3β2 (MII, GIC), α3β4 (AuIB), or α7 (ImI) receptors expressed in *Xenopus* oo-

TABLE III
Comparison of loop II consensus sequences for selected α4/7-conotoxins and analogues
IC_{50} values and selectivity at α7 and α3β2 subtypes expressed in *Xenopus* oocytes are reported.

α-Conotoxin	α3β2	α7	α3β2/α7	Consensus sequence	Reference
	nM	*nM*			
GIC	1.1	n.d.	—	CA**G**NNQ	(45)
PnIA	9.6	252	0.04	CA**A**NNP	(43)
[R12A]GID	10	48	0.2	CA**V**NNO	present study
GID	3.1	4.5	0.7	CR**V**NNO	present study
[A10L]PnIA	99	12.6	7.9	CA**L**NNP	(43)
PnIB	1970	61	32	CA**L**SNP	(43)

cytes (10, 45, 46, 47) (Fig. 1). Other α-conotoxins such as PnIA and PnIB inhibit both the α7 and α3β2 subtypes with nanomolar potencies, with PnIA being α3β2 selective and PnIB being α7 selective (42, 43). GID also has low nanomolar potency at these two nAChR subtypes, but additionally targets the α4β2 receptor at nanomolar levels. Thus GID has structural features that allow it to recognize a broader range of nAChR binding sites than other α-conotoxins, making it a versatile tool for structure-activity studies at the ACh binding site. Comparison of its structure with those of more "specialized" α-conotoxins may reveal the critical determinants for subtype selectivity.

The ACh binding site has been localized at the interface of an α-subunit (+ face) and the respective non-α subunit (or − face in case of the α7 nAChRs) (48–50). To date, there is limited information on the binding mode of neuronally active α-conotoxins and the factors that determine subtype selectivity. In a study to determine the direct interactions between amino acids of the α7 receptor and α-conotoxin ImI, Quiram *et al.* (49) found that the two exposed loops of the peptide interact with different subunits of the α7 receptor, thus bridging the interface between two adjacent subunits. However, a similar mode of binding was not found for PnIB (51). Instead, the key bioactive residues of this peptide form a localized hydrophobic patch that appears to interact mostly with the + face of the α7 binding site. Various neuronally active α-conotoxins might have evolved that have one or more attachment points and target different microdomains that overlap the ACh binding site on nAChRs (51). Therefore, it might be useful to further subgroup the neuronally active α-conotoxins based on their subunit specificity and sequence similarity in order to compare structures that are likely to have similar binding modes.

The three-dimensional solution structure of α-conotoxin GID reveals that it is a well defined molecule, with a backbone RMSD over residues 4–19 of 0.34 Å; however, residues 1–3 are completely disordered. The side-chains are well defined, with the exception of Arg^2, Gla^4, and Arg^{12}. The core of the molecule is occupied by the cysteine residue side-chains, whereas the side-chains of the remaining residues are solvent-exposed. The NMR structure of GID was compared with the crystal structure of PnIA (17), an α-conotoxin with the same global fold and related activity at α7 and α3β2 (Fig. 7*B*). Superimposition of the α-helical backbone residues of GID with PnIA gives an RMS deviation of 0.29 Å. This similarity is evidence that α4/7-conotoxins utilize the same highly conserved, well-defined backbone structure to present a range of different side-chains for interaction with specific nAChRs.

Charge distribution appears to be an important factor that determines nAChR selectivity, with neuronal specific α-conotoxins being neutral or negatively charged, and muscle-specific α-conotoxins having a net positive charge (52). For example, PnIA contains a single negatively charged residue, Asp^{14}, which together with a positive N terminus and neutral, amidated C terminus results in a net charge of zero. At physiological pH, GID has four charged residues including two positive (Arg^2 and Arg^{12}) and two negatively charged residues (Asp^3 and Gla^4). Combined with balancing positive and negatively charged termini (unlike most other conotoxins GID contains no amidated C terminus) the net charge is close to zero. A comparison of the surfaces of GID and PnIA shows that both molecules have a similar hydrophobic patch on one face of the molecule. This patch includes amino acid residues Pro^6, Pro^7, Ala^{10}, and Pro^{13} in PnIA (Fig. 7*B*), and the corresponding residues Pro^9, Ala^{10}, Val^{13}, and O^{16} in GID (Fig. 7*A*). A similar cluster of hydrophobic residues (Leu^5, Pro^6, Pro^7, Ala^9, and Leu^{10}) has been shown to be important for the high affinity binding of PnIB to the α7 receptor (51). Exchanging Ala with Leu at position 10 in PnIA ([A10L]PnIA) enhanced α7 and reduced α3β2 potency, suggesting that a long aliphatic side-chain in this position favored α7 selectivity (42, 43). In support, the α4/7-conotoxin GIC has a Gly in position 10 and is a potent α3β2 inhibitor (45) (see Table III). GID, which has similar potency at both α7 and α3β2 receptors, has an intermediate length side-chain (Val^{13}) in the equivalent position to Ala and Leu. Taken together, it appears that the length of the side-chain in position 10 (or position 13 in GID) of these α4/7-conotoxins correlates with their selectivity for α7 or α3β2 receptors: the longer the aliphatic side-chain the more α7-selective and less α3β2-selective the peptides become (Table III).

The neighboring amino acid residues in positions 9 and 11 also seem to contribute to this selectivity: Arg^{12} of GID (equivalent to Ala^9 of PnIA), contributes to α7 selectivity, since replacing it with an Ala reduced α7 activity by 10-fold without affecting activity at the α3β2 receptor. In contrast, Asn^{11} may contribute more to α3β2 *versus* α7 selectivity, since [N11S]PnIA was 24-fold less active at the α3β2 combination but only 7-fold less active at the α7 subtype as compared with PnIA. Likewise, PnIB, which has a Ser in position 11, was ~20-fold less active at α3β2 receptors but only 5-fold less active at the α7 nAChR than [A10L]PnIA (43). Activity at α7 was little altered in the Asn12Ala and Pro13Hyp analogues of PnIB (51). However, their conservation in most α4/7-conotoxins suggests they have evolved as a structurally important motif. As positions 14 and 15 in PnIB also had little influence on affinity (51), it appears that the side-chains of the first three N-terminal residues in loop II of these α4/7-conotoxins play a key role in determining potency and selectivity at α3β2 and α7 subtypes.

GID contains a unique N-terminal tail comprising four amino acids. Removal of these residues did not affect activity at α7 and α3β2 subtypes but strongly reduced block at the α4β2 subtype, turning GID into a partial inhibitor at this receptor. These results suggest that N-terminal residues outside the cysteine framework can contribute to α4β2 activity. However, this N-terminal motif is not essential for full inhibition of α4β2, since GIC is a full inhibitor of the α4β2 receptor with an IC_{50} value of 300 nM (45). The reduced times to washout of GIDΔ1–4 from the α7 and α3β2 receptors suggest that the N-terminal

tail can stabilize the binding of GID to $\alpha7$ and $\alpha3\beta2$ receptors, presumably by interacting with residues near the ACh binding pocket that are not accessible to smaller α-conotoxins. The reduced activity of [R12A]GID at the $\alpha4\beta2$ receptor indicates that Arg^{12} in loop II also contributes to GID block of $\alpha4\beta2$. Thus GID reveals novel features contributing to α-conotoxin binding to the $\alpha4\beta2$ receptor. Improving the structural stability of the N-terminal tail in GID or adding it to other α-conotoxins provides new avenues for the development of $\alpha4\beta2$ selective inhibitors.

Acknowledgments—We thank Trudy Bond for amino acid analysis, Alun Jones for LC/MS analysis, Roger Pearson for peptide sequencing, and Richard Clark for critical reading of the article.

REFERENCES

1. Lloyd, G. K., and Williams, M. (2000) *J. Pharmacol. Exp. Ther.* **292,** 461–467
2. McGehee, D. S., and Role, L. W. (1995) *Annu. Rev. Physiol.* **57,** 521–546
3. Sargent, P. B. (1993) *Annu. Rev. Neurosci.* **16,** 403–443
4. Elgoyhen, A. B., Vetter, D. E., Katz, E., Rothlin, C. V., Heinemann, S. F., and Boulter, J. (2001) *Proc. Natl. Acad. Sci. U. S. A.* **98,** 3501–3506
5. Colquhoun, L. M., and Patrick, J. W. (1997) *J. Neurochem.* **69,** 2356–2362
6. Sivilotti, L. G., McNeil, D. K., Lewis, T. M, Nassar, M. A., Schoepfer, R., and Colquhoun, D. (1997) *J. Physiol. (Lond.)* **500,** 123–138
7. Dwoskin, L. P., and Crooks, P. A. (2001) *J. Pharmcol. Exp. Ther.* **298,** 395–402
8. McIntosh, J. M., Santos, A. D., and Olivera, B. M. (1999) *Annu. Rev. Biochem.* **68,** 59–88
9. Martinez, J. S., Olivera, B. M., Gray, W. R., Craig, A. G., Groebe, D. R., Abramson, S. N., and McIntosh, J. M. (1995) *Biochemistry* **34,** 14519–14526
10. Johnson, D. S., Martinez, J., Elgoyhen, A. B., Heinemann, S. F., and McIntosh, J. M. (1995) *Mol. Pharmacol.* **48,** 194–199
11. Gehrmann, J., Alewood, P. F., and Craik, D. J. (1998) *J. Mol. Biol.* **278,** 401–415
12. Gehrmann, J., Daly, N. L., Alewood, P. F., and Craik, D. J. (1999) *J. Med. Chem.* **42,** 2364–2372
13. Hill, J. M., Oomen, C. J., Miranda, L. P., Bingham, J. P., Alewood, P. F., and Craik, D. J. (1998) *Biochemistry* **37,** 15621–15630
14. Rogers, J. P., Luginbuhl, P., Shen, G. S., McCabe, R. T., Stevens, R. C., and Wemmer, D. E. (1999) *Biochemistry* **38,** 3874–3882
15. Shon, K. J., Koerber, S. C., Rivier, J. E., Olivera, B. M., and McIntosh, J. M. (1997) *Biochemistry* **36,** 15693–15700
16. Guddat, L. W., Martin, J. A., Shan, L., Edmundson, A. B., and Gray, W. R. (1996) *Biochemistry* **35,** 11329–11335
17. Hu, S. H., Gehrmann, J., Guddat, L. W., Alewood, P. F., Craik, D. J., and Martin, J. L. (1996) *Structure* **4,** 417–423
18. Hu, S. H., Gehrmann, J., Alewood, P. F., Craik, D. J., and Martin, J. L. (1997) *Biochemistry* **36,** 11323–11330
19. Hu, S. H., Loughnan, M., Miller, R., Weeks, C. M., Blessing, R. H., Alewood, P. F., Lewis, R. J., and Martin, J. L. (1998) *Biochemistry* **37,** 11425–11433
20. Cordero-Erausquin, M., Marubio, L. M., Klink, R., and Changeux, J. P. (2000) *Trends Pharmacol. Sci.* **21,** 211–217
21. Schnölzer, M., Alewood, P., Jones, A., Alewood, D., and Kent, S. B. (1992) *Int. J. Pept. Protein Res.* **40,** 180–193
22. Bidlingmeyer, B. A., Cohen, S. A., and Tarvin, T. L. (1984) *J. Chromatogr.* **336,** 93–104
23. Gloor, S., Pongs, O., and Schmalzing, G. (1995) *Gene (Amst.)* **160,** 213–217
24. Nicke, A., Bäumert, H. G., Rettinger, J., Eichele, A., Lambrecht, G., Mutschler, E., and Schmalzing, G. (1998) *EMBO J.* **17,** 3016–3028
25. Marion, D., and Wüthrich, K. (1983) *Biochem. Biophys. Res. Commun.* **113,** 967–974
26. Rance, M., Sorensen, O. W., Bodenhausen, G., Wagner, G., Ernst, R. R., and Wüthrich, K. (1983) *Biochem. Biophys. Res. Commun.* **117,** 479–485
27. Braunschweiler, L., and Ernst, R. R. (1983) *J. Magn. Reson.* **53,** 521–528
28. Bax, A., and Davis, D. G. (1985) *J. Magn. Reson.* **56,** 355–360
29. Griesinger, C., Sorensen, O. W., and Ernst, R. R. (1987) *J. Magn. Reson.* **75,** 474–492
30. Jeener, J., Meier, B. H., Bachmann, P., and Ernst, R. R. (1979) *J. Chem. Phys.* **71,** 4546–4553
31. Piotto, M., Saudek, V., and Sklenar, V. (1992) *J. Biomol. NMR* **2,** 661–665
32. Eccles, C., Guntert, P., Billeter, M., and Wüthrich, K. (1991) *J. Biomol. NMR* **1,** 111–130
33. Wüthrich, K. (1986) *NMR of Proteins and Nucleic Acids*, Wiley-Interscience, New York
34. Guntert, P., Mumenthaler, C., and Wüthrich, K. (1997) *J. Mol. Biol.* **273,** 283–298
35. Koradi, R., Billeter, M., and Wüthrich, K. (1996) *J. Mol. Graph.* **14,** 51–55:29–32
36. Brünger, A. T., Adams, P. D., and Rice, L. M. (1997) *Structure* **5,** 325–336
37. Rice, L. M., and Brünger, A. T. (1994) *Proteins* **19,** 277–290
38. Stein, E. G., Rice, L. M., and Brünger, A. T. (1997) *J. Magn. Reson.* **124,** 154–164
39. Linge, J. P., and Nilges, M. (1999) *J. Biomol. NMR* **13,** 51–59
40. Hutchinson, E. G., and Thornton, J. M. (1996) *Protein Sci.* **5,** 212–220
41. Laskowski, R. A., Rullmannn, J. A., MacArthur, M. W., Kaptein, R., and Thornton, J. M. (1996) *J. Biomol. NMR* **8,** 477–486
42. Hogg, R. C., Miranda, L. P., Craik, D. J., Lewis, R. J., Alewood, P. F., and Adams, D. J. (1999) *J. Biol. Chem.* **274,** 36559–36564
43. Luo, S., Nguyen, T. A., Cartier, G. E., Olivera, B. M., Yoshikami, D., and McIntosh, J. M. (1999) *Biochemistry* **38,** 14542–14548
44. Wishart, D. S., Bigam, C. G., Holm, A., Hodges, R. S., and Sykes, B. D. (1995) *J. Biomol. NMR* **5,** 67–81
45. McIntosh, J. M., Dowell, C., Watkins, M., Garret, J. E., Yoshikami, D., and Olivera, B. M. (2002) *J. Biol. Chem.* **277,** 33610–33615
46. Cartier, G. E., Yoshikami, D., Gray, W. R., Luo, S., Olivera, B. M., and McIntosh, J. M. (1996) *J. Biol. Chem.* **271,** 7522–7528
47. Luo, S., Kulak, J. M., Cartier, G. E., Jacobsen, R. B., Yoshikami, D., Olivera, B. M., and McIntosh, J. M. (1998) *J. Neurosci.* **18,** 8571–8579
48. Hucho, F., Tsetlin, V. I., and Machold, J. (1996) *Eur. J. Biochem.* **239,** 539–557
49. Quiram, P. A., Jones, J. J., and Sine, S. M. (1999) *J. Biol. Chem.* **274,** 19517–19524
50. Karlin, A. (2002) *Nat. Rev. Neurosci.* **3,** 102–114
51. Quiram, P. A., McIntosh, J. M., and Sine, S. M. (2000) *J. Biol. Chem.* **275,** 4889–4896
52. Rogers, J. P., Luginbuhl, P., Pemberton, K., Harty, P., Wemmer, D. E., and Stevens, R. C. (2000) *J. Mol. Biol.* **304,** 911–926
53. Loughnan, M., Bond, T., Atkins, A., Cuevas, J., Adams, D. J., Broxton, N., Livett, B., Down, J., Jones, A., Alewood, P. F., and Lewis, R. J. (1998) *J. Biol. Chem.* **273,** 15667–15674

Isolation, Structure, and Activity of GID, a Novel α4/7-Conotoxin with an Extended N-terminal Sequence

Annette Nicke, Marion L. Loughnan, Emma L. Millard, Paul F. Alewood, David J. Adams, Norelle L. Daly, David J. Craik and Richard J. Lewis

J. Biol. Chem. 2003, 278:3137-3144.
doi: 10.1074/jbc.M210280200 originally published online November 4, 2002
